Watari *Earth, Planets and Space* (2017) 69:70
DOI 10.1186/s40623-017-0653-z

Earth, Planets and Space

LETTER Open Access

Geomagnetic storms of cycle 24 and their solar sources

Shinichi Watari*

Abstract

Solar activity of cycle 24 following the deep minimum between cycle 23 and cycle 24 is the weakest one since cycle 14 (1902–1913). Geomagnetic activity is also low in cycle 24. We show that this low geomagnetic activity is caused by the weak dawn-to-dusk solar wind electric field (E_{d-d}) and that the occurrence rate of $E_{d-d} > 5$ mV/m decreased in the interval from 2013 to 2014. We picked up seventeen geomagnetic storms with the minimum Dst index of less than −100 nT and identified their solar sources in cycle 24 (2009–2015). It is shown that the relatively slow coronal mass ejections contributed to the geomagnetic storms in cycle 24.

Keywords: Geomagnetic storm, Rising and maximum phases, Two peaks, Solar cycle 24, Coronal mass ejection, Coronal hole

Introduction

The solar minimum period between cycle 23 and cycle 24 was the lowest and the longest one since the minimum between cycle 14 and cycle 15, and is called as the 'deep minimum' (Russell et al. 2010; Richardson and Cane 2012a; Richardson 2013; McComas et al. 2013). The solar activity of the current solar cycle (No. 24), following the extraordinary low minimum, is also low (Kamide and Kusano 2013; Gopalswamy et al. 2014; Watari et al. 2015). The maximum of cycle 24, determined by the 13-month smoothed monthly sunspot number (SSN), occurred in April 2014. The maximum SSN was 116.4 according to the World Data Center for Sunspot Index and Long-term Solar Observation (WDC-SILSO), Royal Observatory of Belgium, Brussels. This is the smallest one ever observed since the maximum of cycle 14 (SSN of 107.1 in February 1906). The SSNs of cycle 24 show two peaks: 98.3 in March 2012 and 116.4 in April 2014 (Svalgaard and Kamide 2013; Gopalswamy et al. 2015). On a two-peak variation of geomagnetic activities seen in past solar cycles, Gonzalez et al. (1990) and Echer et al. (2011) noted that the first peak, appearing in the maximum phase, is caused by coronal mass ejections (CMEs) and the second peak, appearing in the declining phase, is caused by high-speed streams from coronal holes. Gopalswamy (2008) pointed out latitudinal distribution of CMEs had a close connection to the two-peak characteristics of geomagnetic activities.

To study the nature of the weak activity of cycle 24, we examined long-term variations of geomagnetic activities, expressed by the Dst index, comparing with the SSNs and the solar wind data. We also investigated the solar sources of the geomagnetic storms in the rising and the maximum phases of cycle 24 using the solar and the solar wind data.

There are numerous studies on geomagnetic storms and their solar sources in past cycles (Zhang et al. 2007; Echer et al. 2008, 2011; Richardson et al. 2006; Richardson and Cane 2012a, b; references therein). According to the previous studies, the principal solar sources of intense geomagnetic storms (minimum Dst < −100 nT) were identified to be CMEs and approximately 11–14% of the storms were associated with high-speed streams from coronal holes (see Fig. 4 in Zhang et al. (2007) and Fig. 10 in Echer et al. (2008)). We will compare these results of the previous cycles with our study of cycle 24.

Data sources

We used the Dst index data, provided by the WDC for Geomagnetism, Kyoto, as the parameter of the level of

*Correspondence: watari@nict.go.jp
National Institute of Information and Communications Technology, 4-2-1 Nukuikita, Koganei, Tokyo 184-8795, Japan

geomagnetic activity. There are three categories: the real-time, the provisional, and the final indices. The real-time Dst is derived from the unverified raw data. The provisional Dst is calculated using the data visually screened for artificial noises. The WDC provides the final Dst between 1957 and 2011 and the provisional Dst between 2012 and 2014 and for March 2015 at the time of this analysis. Long-term variation of geomagnetic activity, represented by the Dst data, will be compared with the SSN data, provided by the WDC-SILSO, and the NASA/OMNI solar wind data (http://omniweb.gsfc.nasa.gov).

Data analysis and discussion

Long-term variation of geomagnetic activity since 1957

Because the comprehensive dataset of the Dst index is available since 1957, we can see the long-term correlation characteristics between solar and geomagnetic activities in the interval including six solar maxima. Figure 1 shows the yearly and the 13-month smoothed monthly SSNs and occurrence rates of the daily minimum Dst of less than −100, −200, and −300 nT, respectively for each year. The smoothed curve of the monthly SSNs of cycle 24 shows a peak in 2012 and 2014, respectively. Also seen in this figure is a decrease of the geomagnetic activity (Dst < −100 nT) in 2013–2014. This decrease reflects a decreasing tendency of the number of halo CMEs in 2013 and 2014 as noted by Gopalswamy et al. (2015). Cycle 22 also shows two peaks of SSNs taking place in 1989 and in 1991, respectively, and there is a decrease of the geomagnetic activity (Dst < −100 nT) between these peaks, namely in 1990.

Correlation between geomagnetic activity and SSN

According to Fig. 1, the level of the geomagnetic activity tends to be proportional to that of the solar activity. Figure 2 shows scatter plots of occurrence rates of the daily minimum Dst of less than −50, −100, −200, and −300 nT, respectively for each year, against the yearly averaged SSNs. For the data points in each panel for the Dst of <−50, <−100, and <−200 nT, respectively, in Fig. 2, we can see the presence of an upper border line having the positive inclination, namely the occurrence rate tends to be increased with respect to the yearly SSN. Similar tendency can be seen also in the case of strong geomagnetic activities (Dst < −300 nT) because the 'no-event' points are nested in the low SSN part of the diagram.

Correlation between geomagnetic activity and solar wind electric field

It is known that the rate of energy injection into the magnetospheric ring current, affecting change of Dst, is a function of the dawn-to-dusk solar wind electric field, E_{d-d} (Burton et al. 1975; O'Brien and McPherron 2000). Figure 3 shows scatter plots of the daily minimum of Dst versus the daily maximum E_{d-d} in the rising–maximum phases of cycle 23 (1996–2002) and cycle 24 (2009–2015). In this analysis, we use the 1-h averaged solar wind data since 1996 because the time resolution of Dst is 1 h and coverage of the solar wind data is approximately 100% since this year.

The number of the data points of Dst < −100 nT and E_{d-d} > 5 mV/m is 60 points in cycle 23 and 18 points in cycle 24. E_{d-d} of larger than 20 mV/m or Dst of less than −250 nT were not observed in the rising–maximum phases of cycle 24. It is also seen in Fig. 3 that there exists a remarkable tendency in the cases of strong electric fields or strong geomagnetic storms. This scattering tendency is produced by the data points obtained in the growth or the recovery phase of individual geomagnetic storms. For example, the data point corresponding to $E_{d-d} = 14.3$ mV/m and Dst = −118 nT in the right panel of Fig. 3 is associated with the shock and the sheath of a CME, which was identified to be the source of the 26 September 2011 storm. On the other hand, the data point of $E_{d-d} = 17.8$ mV/m and Dst = −121 nT in the right panel of Fig. 3 is associated with the growth phase of the 22 June 2015 storm.

Figure 4, respectively, shows the yearly and the 13-month smoothed monthly SSNs (the top panel) and the occurrence rates of $|E_{d-d}| > 5$ mV/m (the second panel), of $E_{d-d} > 5$ mV/m (the third panel), and of $E_{d-d} < -5$ mV/m (the forth panel) in the 1-h averaged solar wind data of the year. The bottom panel shows yearly occurrence ratios of $E_{d-d} < -5$ mV/m to $|E_{d-d}| > 5$ mV/m. The occurrence rates of $|E_{d-d}| > 5$ mV/m in the rising–maximum phases of cycle 24 are generally smaller than those in the same phase of cycle 23 and the occurrence rate of $E_{d-d} > 5$ mV/m decreased in 2013–2014. The averaged ratio of $E_{d-d} < -5$ mV/m to $|E_{d-d}| > 5$ mV/m enhanced remarkably in 2014, namely in the maximum phase of cycle 24, probably due to an increase of the number of magnetic clouds with fields rotating north–south (NS-type) in even cycles. Bothmer and Rust (1997) noted that the NS-type magnetic clouds are expected to be observed more frequently in even solar cycles than in odd cycles. Northward magnetic field of front-side of the NS-type magnetic clouds tends to be strengthened by compression during their propagation from Sun to Earth. This will increase the occurrence rate of the strong positive electric filed. On the other hand, Kilpua et al. (2012) pointed out that there is no obvious difference in the geo-effectiveness between SN-type and NS-type magnetic clouds. To examine the difference of solar wind characteristics controlling E_{d-d}, we analysed solar wind parameters related to E_{d-d} in the following subsection.

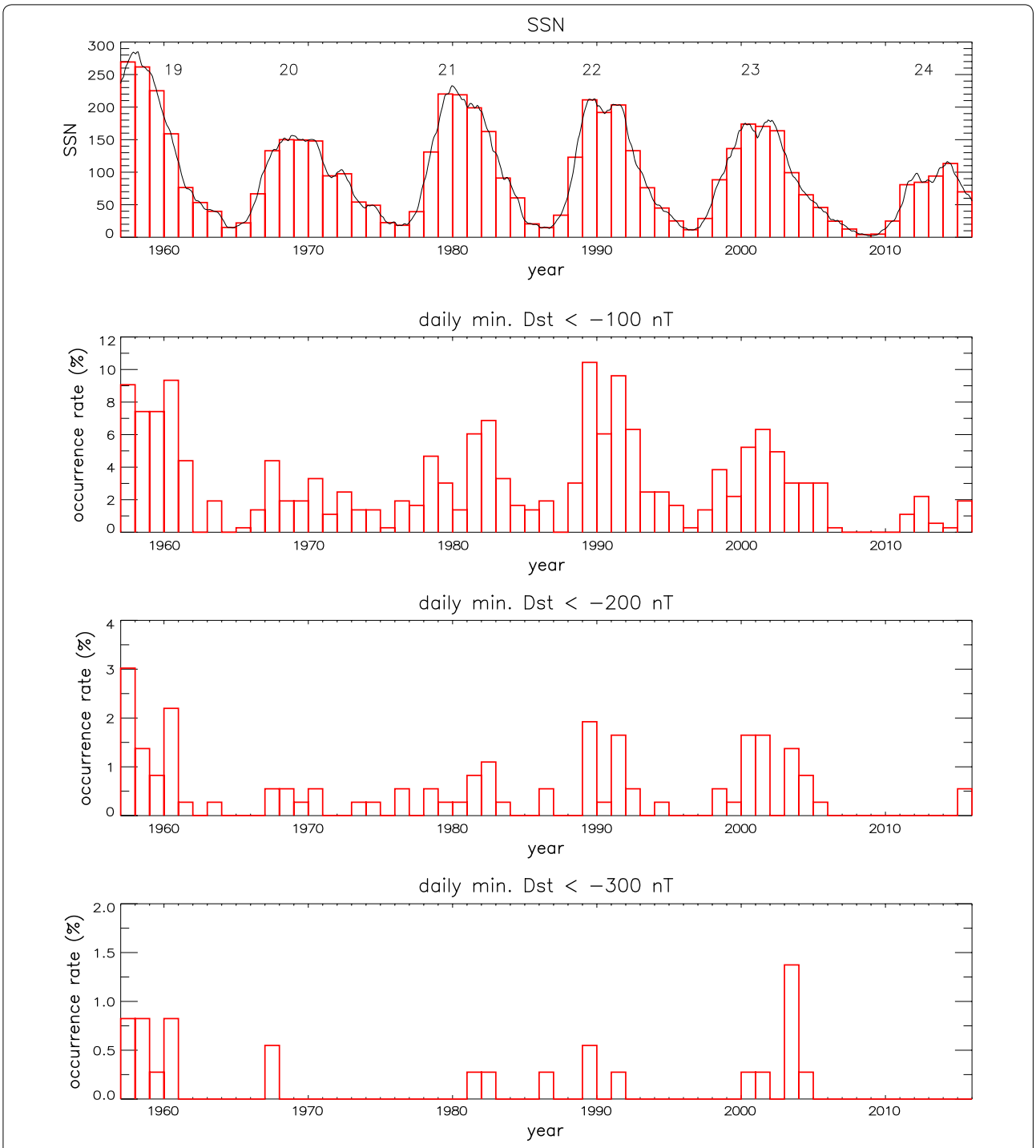

Fig. 1 *Top panel* is the yearly SSNs (*red line*) with the 13-month smoothed monthly SSNs (*black line*). The *second*, *third*, *fourth panels* show yearly occurrence rates of the daily minimum Dst of less than −100, −200, and −300 nT, respectively

Correlation between E_{d-d} and solar wind parameters

The E_{d-d} is given by a product of the solar wind speed (V) and the north–south component of solar wind magnetic field (Bz). Figure 5 shows scatter plots of Bz versus V in the rising–maximum phases of cycle 23 (1996–2002) and cycle 24 (2009–2015). Doted curves in the plots show E_{d-d} of ±5, ±10, ±15, and ±20 mV/m, respectively.

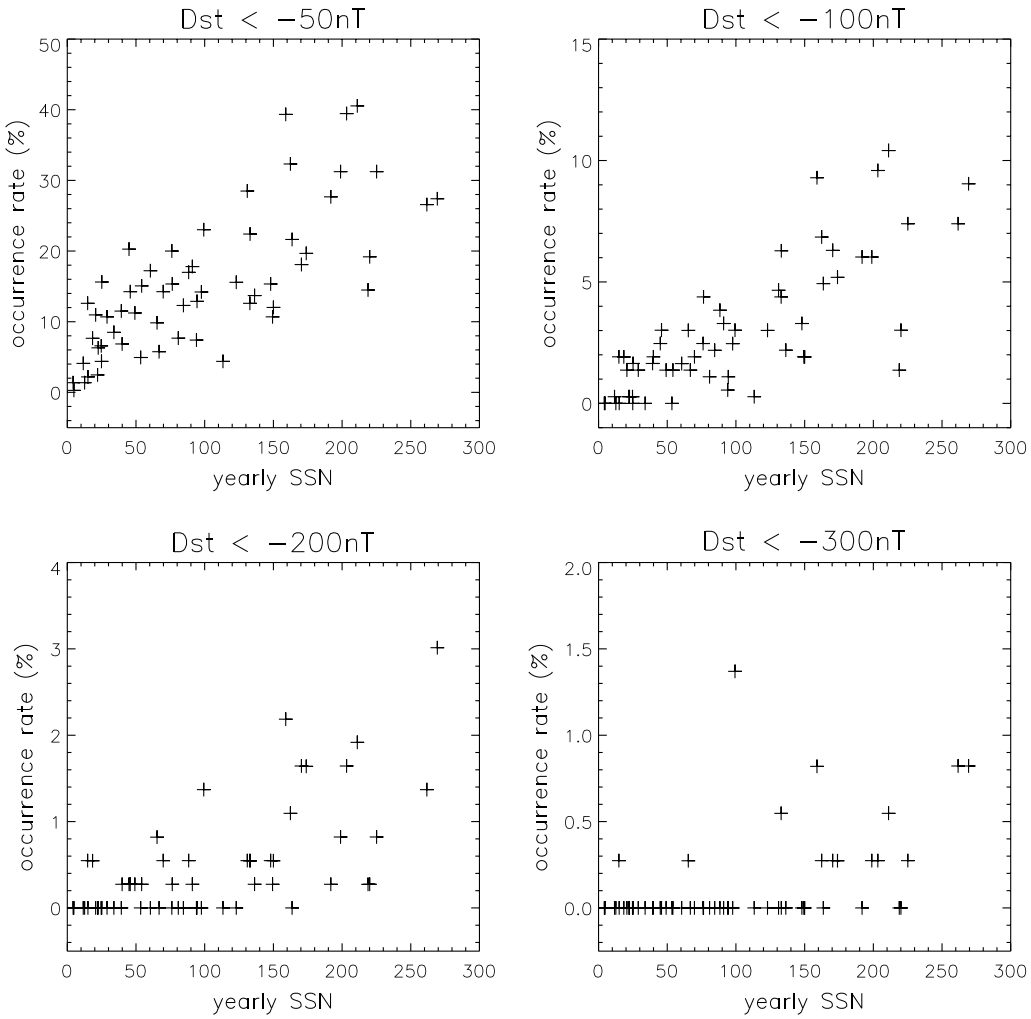

Fig. 2 Yearly SSNs and the yearly occurrence rates of the daily minimum Dst of less than −50, −100, −200, and −300 nT, respectively

The number of data points (193) corresponding to the cases of $E_{d-d} > 5$ mV/m in cycle 24 is smaller than that (415) in cycle 23, and no data point can be seen in the area of both $V > 750$ km/s and Dst < -10 nT in cycle 24. This suggests that the solar wind disturbances associated with geomagnetic storms in cycle 24 are weaker than those in cycle 23. Averaged V and Bz for the data points corresponding to $E_{d-d} > 5$ mV/m are 532 km/s and −14 nT for cycle 23, and 503 km/s and −14 nT for cycle 24, respectively.

Geomagnetic storms in the rising–maximum phases of cycle 24

We selected seventeen geomagnetic storms with the minimum Dst of less than −100 nT in the list of geomagnetic storms (2009–2015) provided from the Kakioka Magnetic Observatory, the Japan Meteorological Agency (http://www.kakioka-jma.go.jp/obsdata/metadata/en/products/list/event/kak). Their solar sources are identified using the NASA/OMNI solar wind data and the solar data obtained by the Solar and Heliosphere Observatory (SOHO)/the Large Angle and Spectrometric Coronagraph (LASCO) (ESA/NASA) and by the Solar Dynamics Observatory (SDO)/Atmospheric Imaging Assembly (AIA) (NASA, http://sdo.gsfc.nasa.gov/).

Table 1 shows characteristics of the selected geomagnetic storms with information on their solar sources. The most intense geomagnetic storm in the rising–maximum phases of cycle 24 is the 17 March 2015 storm, currently called as 'the St. Patrick's Day storm', with the minimum Dst index of −223 nT (Kamide and Kusano 2015). Kataoka et al. (2015) noted that this storm was intensified by

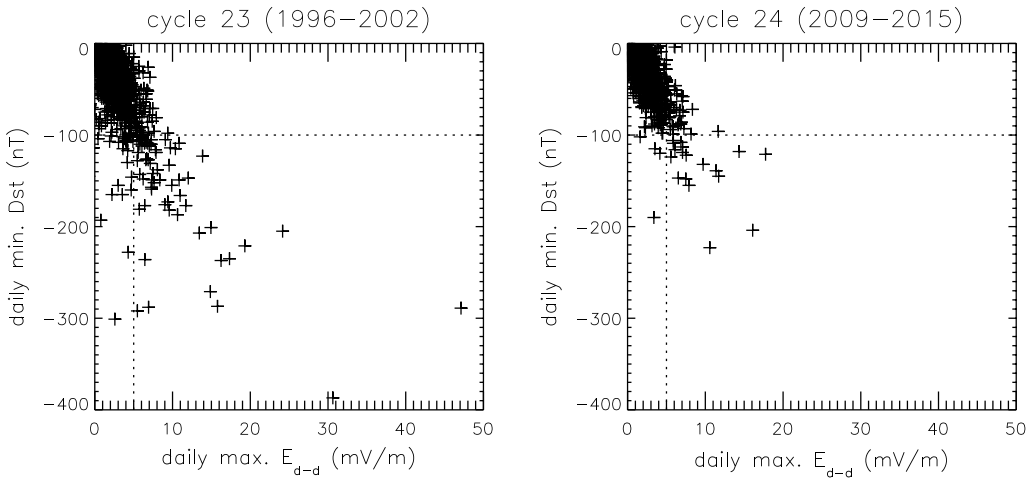

Fig. 3 Daily maximum dawn-dusk solar wind electric fields (E_{d-d}) and the daily minimum Dst for the rising–maximum phases of cycle 23 (1996–2002, the *left panel*) and cycle 24 (2009–2015, the *right panel*). The *horizontal dotted line* shows the daily minimum Dst of −100 nT, and the *vertical dotted line* shows the daily maximum E_{d-d} of 5 mV/m

interaction of a CME and following high-speed stream shortly before its arrival at the Earth. According to Table 1, occurrence of the geomagnetic storms in cycle 24 showed two-peak characteristics. There are six storms in 2012 and five storms in 2015, but only three storms occurred between 2013 and 2014.

Also seen in Table 1 is that the geomagnetic storms were mainly caused by CMEs in the studied period of cycle 24 and that relatively slow CMEs contributed to the geomagnetic storms. Two geomagnetic storms in this table were mainly produced by high-speed solar wind from coronal holes.

Summary

We made a comprehensive data analysis of long-term variations of geomagnetic activities with the SSNs and the solar wind data to investigate characteristics of the low geomagnetic activity of cycle 24. We identified the solar sources of the geomagnetic storms in the rising–maximum phases of cycle 24 using the solar and the solar wind data. Geomagnetic activity of the studied period of cycle 24 (2009–2015) was in the lowest level in the recent six solar cycles since 1957. There were only seventeen geomagnetic storms (minimum Dst < −100 nT). The results of our analysis are summarized below.

1. There is an upper limit of the yearly occurrence rate of the geomagnetic activities for a given SSN. The level of the limit is approximately proportional to the yearly SSN.
2. The storm time daily minimum Dst is approximately proportional to the daily maximum value of E_{d-d}.
3. The occurrence rate of $|E_{d-d}|$ of larger than 5 mV/m in cycle 24 is lower than the occurrence rate in cycle 23 and the occurrence rate of $E_{d-d} > 5$ mV/m decreased in 2013–2014. The averaged ratio of $E_{d-d} < -5$ mV/m to $|E_{d-d}| > 5$ mV/m enhanced remarkably in 2014.
4. Concerning the 1-h averaged solar wind data in the rising–maximum phases of cycle 24, no data point of Bz < −10 nT is recorded in the cases of $V > 750$ km/s. For the cases of $E_{d-d} > 5$ mV/m, averaged V and Bz of the data points ($E_{d-d} > 5$ mV/m) are 532 km/s and −14 nT for cycle 23, and 503 km/s and −14 nT for cycle 24, respectively.
5. Geomagnetic activities in cycle 24 showed two-peak characteristics.
6. The geomagnetic storms in the studied period of cycle 24 were mainly caused by CMEs. Only two storms have been identified to be associated with high-speed solar wind from coronal holes. The rate of solar sources is similar to those of other cycles estimated by Zhang et al. (2007) and Echer et al. (2008).

We need to continuously watch geomagnetic activity in declining-minimum phase of cycle 24 for further understanding of this weak cycle.

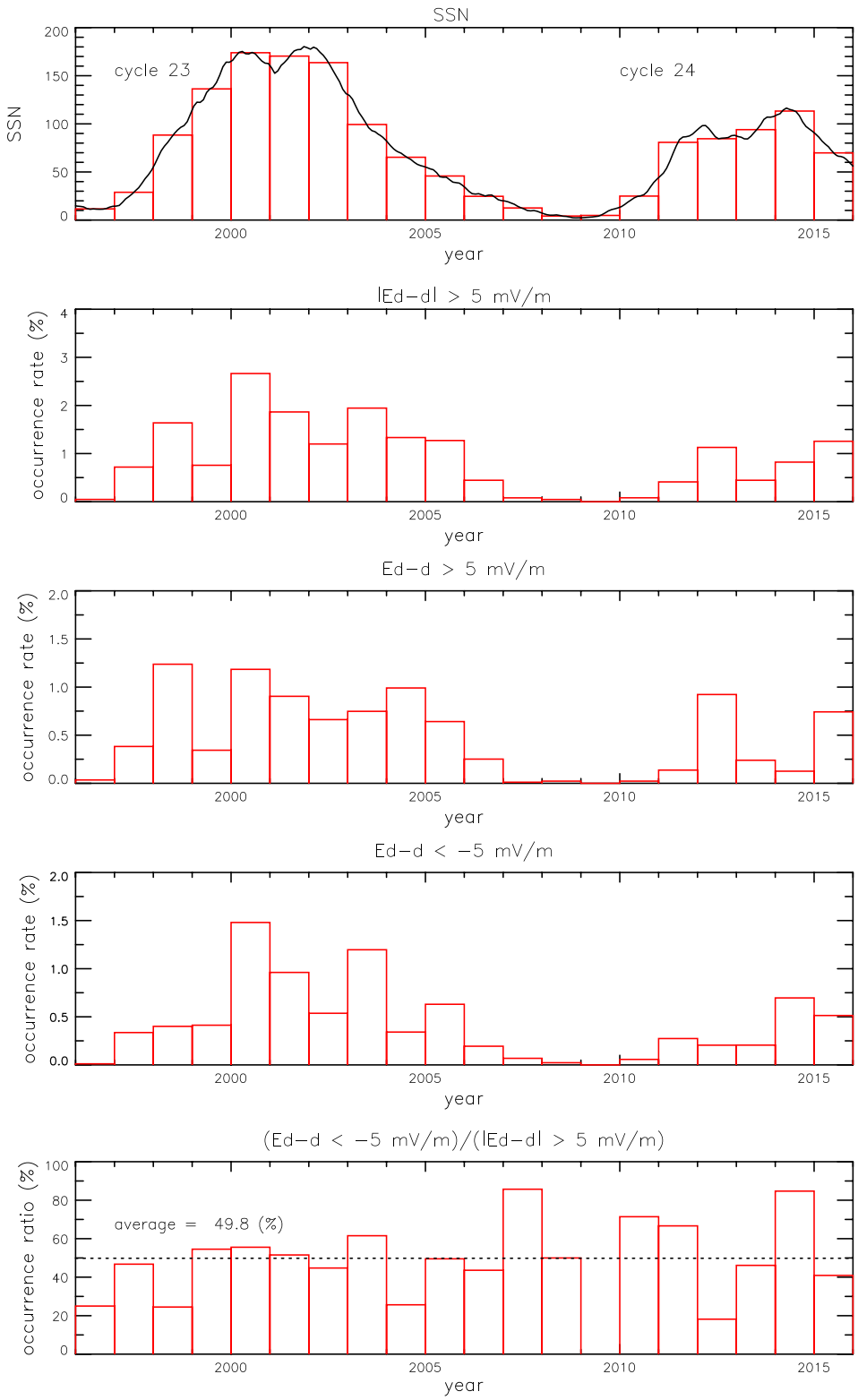

Fig. 4 *Top panel* is the yearly SSNs (*red line*) with the 13-month smoothed monthly SSNs (*black line*). The *second*, *third*, and *forth panels* are the yearly occurrence rates of $|E_{d-d}| > 5$ mV/m, of $E_{d-d} > 5$ mV/m, and of $E_{d-d} < -5$ mV/m in the 1-year data. The *bottom panel* is yearly occurrence ratios of $E_{d-d} < -5$ mV/m to $|E_{d-d}| > 5$ mV/m

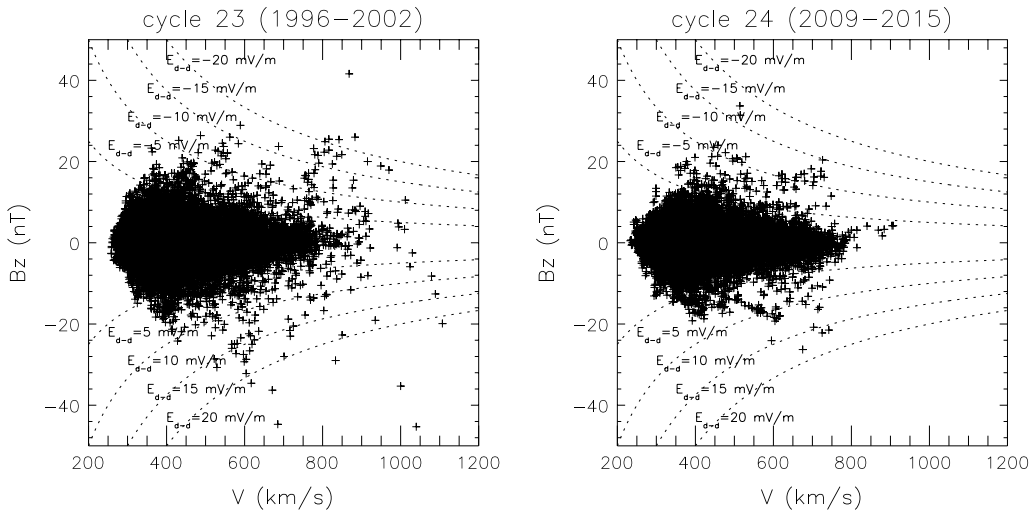

Fig. 5 Scatter plots of the 1-h averaged solar wind speed (*V*) and the north–south component of solar wind magnetic field (Bz). The *left panel* is for the rising–maximum phases of cycle 23 (1996–2002), and the *right panel* is for cycle 24 (2009–2015). The *dotted curves* show E_{d-d} of ±5, ±10, ±15, and ±20 mV/m, respectively

Table 1 Geomagnetic storms (minimum Dst < −100 nT) in the rising–maximum phases of cycle 24 with their characteristics

No.	Date	Min. Dst (nT)	Type	Solar sources	Speed at 1AU (km/s)
1	2011/08/05 17:50–2011/08/06 15:00	−115[*1]	SC	Full halo CME (sheath)	611
2	2011/09/26 12:35–2011/09/28 17:00	−118[*1]	SC	Full halo CME (sheath)	704
3	2011/10/24 18:31–2011/10/25 21:00	−147[*1]	SC	Full halo CME (sheath, MC)	534
4	2012/03/08 11:03–2012/03/10 19:00	−145[*2]	SC	Full halo CME (sheath, MC) multiple	737
5	2012/04/23 03:20–2012/04/26 16:00	−120[*2]	SC	Partial halo CME (sheath, MC)	394/720
6	2012/07/14 18:10–2012/07/17 12:00	−139[*2]	SC	Full halo CME (sheath, MC)	667
7	2012/09/30 11:32/23:05–2012/10/01 16:00	−122[*2]	SC	Full halo CMEs (sheath, MC) multiple	410
8	2012/10/08 05:16–2012/10/09 24:00	−109[*2]	SC	Partial halo CME (sheath, MC) multiple	447/526
9	2012/11/12 23:12–2012/11/14 19:00	−108[*2]	SC	Partial halo CME (sheath, MC) multiple	467
10	2013/03/17 06:00–2013/03/18 12:00	−132[*2]	SC	Full halo CME (sheath, MC) multiple	725
11	2013/05/31 16:17–2013/06/02 21:00	−119[*2]	SC	(MC?) coronal hole	402/774
12	2014/02/18 13:54–2014/02/19 23:00	−116[*2]	GC	Partial halo CME (MC) multiple	530
13	2015/03/17 04:45–2015/03/21 15:00	−223[*2]	SC	Partial halo CME (sheath, MC) coronal hole?	683
14	2015/06/22 18:33–2015/06/24 12:00	−204[*3]	SC	Full halo CME (sheath, MC) multiple	742
15	2015/10/07 04:24–2015/10/10 02:00	−124[*3]	GC	(MC) coronal hole	460/775
16	2015/12/19 16:17–2015/12/22 02:00	−155[*3]	SC	Full halo CME (MC)	497
17	2015/12/31 00:49–2016/01/01 16:00	−110[*3]	SC	Partial halo CME (MC)	485

SC sudden commencement, *GC* gradual commencement, *MC* magnetic cloud

[*1] Final Dst index

[*2] Provisional Dst index

[*3] Real-time Dst index

Acknowledgements
We thank the Kakioka Magnetic Observatory for the list of geomagnetic storms, the WDC for Geomagnetism, Kyoto, for the Dst index data, and the WDC-SILSO for the SSN data, the SDO/AIA data and the OMNI solar wind data for NASA, the SOHO/LASCO data for ESA and NASA. This work was supported by JSPS KAKENHI Grant Number 15H05815.

Competing interests
The author declares that he has no competing interests.

Publisher's Note

Received: 30 April 2016 Accepted: 12 May 2017
Published online: 19 May 2017

References

Bothmer V, Rust DM (1997) The field configuration of magnetic clouds and the solar cycle. In: Crooker N, Joselyn JA, Feynman J (eds) Coronal mass ejections. Geophysical monograph. AGU, Washington

Burton RK, McPherron RL, Russell CT (1975) An empirical relationship between interplanetary conditions Dst. J Geophys Res 80(31):4204–4214

Echer E, Gonzalez WD, Tsurutani BT, Gonzalez LC (2008) Interplanetary conditions causing intense geomagnetic storms (Dst ≤ -100 nT) during solar cycle 23 (1996–2006). J Geophys Res 113:A052221. doi:10.1029/2007JA012744

Echer E, Gonzalez WD, Tsurutani BT (2011) Statistical studies of geomagnetic storms with peak Dst ≤ -50 nT from 1957 to 2008. J Atmos Sol Terr Phys 73(11–12):1454–1459. doi:10.1016/j.jastp.2011.04.21

Gonzalez WD, Gonzalez ALC, Tsurutani BT (1990) Dual-peak solar cycle distribution of intense geomagnetic storms. Planet Space Sci 38(2):181–187

Gopalswamy N (2008) Solar connections of geoeffective magnetic structures. J Atmos Sol Terr Phys 70(17):2078–2100. doi:10.1016/j.jastp.2008.06.010

Gopalswamy N, Xie H, Akiyama S, Makela PA, Yashiro S (2014) Major solar eruptions and high-energy particle events during solar cycle 24. Earth Planets Space 66:104. doi:10.1186/1880-5981-66-104

Gopalswamy N, Makela P, Akiyama S, Yashiro S, Thakur N (2015) CMEs during the two peaks in cycle 24 and their space weather consequences. Sun Geosph 10(2):111–118

Kamide Y, Kusano K (2013) Is something wrong with the present solar maximum? Space Weather 11:140–1411. doi:10.1002/ewe.20045

Kamide Y, Kusano K (2015) No major solar flares but the largest geomagnetic storm in the present solar cycle. Space Weather 13:365–367. doi:10.1002/2015SW001213

Kataoka R, Shiota D, Kilpua E, Keika K (2015) Pileup accident hypothesis of magnetic storm on 17 March 2015. Gephys Res Lett 42:5155–5156. doi:10.1002/215GL064816

Kilpua EKJ, Li Y, Luhmann JG, Jian LK, Russell CT (2012) On the relationship between magnetic cloud field polarity and geoeffectiveness. Ann Geophys 30:1037–1050. doi:10.5194/angeo-30-1037-2012

McComas DJ, Angold N, Elliott HA, Livadiotis G, Schwadron NA, Skoug RM, Smith CW (2013) Weakest solar wind of the space age and the current "Mini" solar maximum. Astrophys J. doi:10.1088/0004-637X/779/1/2

O'Brien TP, McPherron L (2000) Forecasting the ring index Dst in real time. JASTP 62:1295–1299

Richardson IG (2013) Geomagnetic activity during the rising phase of solar cycle 24. J. Space Weather Space Clim. 3:A08. doi:10.1051/swsc/2013031

Richardson IG, Cane HV (2012a) Solar wind driver of geomagnetic storms during more than four solar cycles. J. Space Weather Space Clim 2:A01. doi:10.1051/swsc/2012001

Richardson IG, Cane HV (2012b) Near-Earth solar wind flows and related geomagnetic activity during more than dour solar cycles (1963–2011). J Space Weather Space Clim 2:A02. doi:10.1051/swsc/2013003

Richardson IG, Webb DF, Zhang J, Berdichevsky DB, Biesecker DA, Kasper JC, Kataoka R, Steinberg JT, Thompson BJ, Wu C-C, Zhukov AN (2006) Solar and interplanetary sources of major geomagnetic storms (Dst ≤ -100nT) generated by corotating interaction regions. J Geophys Res 111:A07S09. doi:10.1029/2005JA011476

Russell CT, Luhmann JG, Jian LK (2010) How unprecedented a solar minimum? Rev Geophys 48:RG2004. doi:10.1029/2009RG000316

Svalgaard L, Kamide Y (2013) Asymmetric solar polar field reversal. Astrophys J. doi:10.1088/0004-637X/763/1/23

Watari S, Kato H, Yamamoto K (2015) Hit rate of space weather forecasts of the Japanese forecast center and analysis of problematic events on the forecasts between June 2014 and March 2015. Sun Geosph 10(2):163–171

Zhang J, Richardson IG, Webb DF, Gopalswamy N, Huttunen E, Kasper JC, Nitta NV, Poomvises W, Thompson BJ, Wu C-C, Yashiro S, Zhukov AN (2007) Solar and interplanetary sources of major geomagnetic storms (Dst ≤ -100 nT) during 1996–2005. J Geophys Res 112:A10102. doi:10.1029/2007JA012321